Article:

Potts, J. orcid.org/0000-0002-8564-2904 and Lewis, M.A. (2016) How memory of direct animal interactions can lead to territorial pattern formation. Interface, 13 (118). 20160059. ISSN 1742-5689

https://doi.org/10.1098/rsif.2016.0059

Supplementary Information for 'How memory of ritualised aggression can lead to territorial pattern formation'

Jonathan R. Potts[1,a], Mark A. Lewis[2,3,b]

1 School of Mathematics and Statistics, University of Sheffield, UK

2 Centre for Mathematical Biology, Department of Mathematical and Statistical Sciences, 632 CAB, University of Alberta, Canada, T6G 2G1.

3 Department of Biological Sciences, University of Alberta, Edmonton, Canada

a E-mail: j.potts@sheffield.ac.uk. Phone: +44(0)114-222-3729.

b E-mail: mark.lewis@ualberta.ca.

Supplementary Appendix A

Here, we explain how to move from a description of the 1D system's dynamics in discrete space and time (Equations 1 and 3 from the Main Text) to the continuum PDE model (Equations 4 and 5 from the Main Text).

A.1 The conflict zone

Let $U_i(n,s)$ be the probability of agent i being at lattice site n at time-step s and $\langle K_i(n,s)\rangle$ be the expectation of $K_i(n,s)$. Then, taking expectations on each side of Equation (1) from the Main Text, and neglecting covariances (i.e. taking a mean-field approximation), we find

$$\begin{aligned}
\langle K_i(n,s+1)\rangle =&(1-\mu\tau)\rho_{\tau,l}U_1(n,s)U_2(n,s)\\
&+[1-\rho_{\tau,l}U_1(n,s)U_2(n,s)]U_i(n,s)[1-(\mu+\beta_l)\tau]\langle K_i(n,s)\rangle\\
&+[1-\rho_{\tau,l}U_1(n,s)U_2(n,s)][1-U_i(n,s)](1-\mu\tau)\langle K_i(n,s)\rangle\\
=&(1-\mu\tau)\rho_{\tau,l}U_1(n,s)U_2(n,s)\\
&+[1-\rho_{\tau,l}U_1(n,s)U_2(n,s)]\langle K_i(n,s)\rangle[1-\mu\tau-U_i(n,s)\beta_l\tau]
\end{aligned} \tag{1}$$

Now we take the continuum limit, using $x = nl$ and $t = s\tau$ to denote continuous space and time respectively. Let $k_i(x,t)$ be the probability that position x is part of the conflict zone at time t and $u_i(x,t)$ be the position probability density for agent i at time t. Taking the limit as $l,\tau \to 0$ and $\beta_l, n, s \to \infty$ such that $x = nl$, $t = s\tau$, $\rho = \rho_{\tau,l}l^2/\tau$, and $\beta = l\beta_l$ remain constant, we arrive at the following differential equation describing the evolution of the conflict zone

$$\frac{\partial k_i}{\partial t} = \rho u_1 u_2(1-k_i) - k_i(\mu + u_i\beta), \tag{2}$$

dropping the explicit dependence of k_i and u_i on x and t for ease of notation.

A.2 A model of agent movement

To find a continuous space-time description of agent movement, we start by using the movement kernel from Equation (3) from the Main Text to describe how the probability distribution, $U_i(n,s)$ of agent i evolves over time. This is done via the following master equation

$$
\begin{aligned}
U_i(n,s+1) &= \sum_{n' \in \Omega} U_i(n',s) f_i(n|n',h,d) \\
&= \frac{1}{2} U_i(n-1,s) \left[1 + q\bar{K}_i(n+2d,s|h) - q\bar{K}_i(n,s|h)\right] \\
&+ \frac{1}{2} U_i(n-1,s) \left[1 - q\bar{K}_i(n,s|h) + q\bar{K}_i(n-2d,s|h)\right]. \qquad (3)
\end{aligned}
$$

Equation (3) rearranges to give the following equation

$$
\begin{aligned}
\frac{U_i(n,s+1) - U_i(n,s)}{\tau} = \frac{l^2}{2\tau} \Bigg\{ & \frac{U_i(n+1,s) - 2U_i(n,s) + U_i(n-1,s)}{l^2} \\
& + 4dq \frac{1}{2l} \Bigg[U_i(n+1,s) \frac{\bar{K}_i(n+2d,s|h) - \bar{K}_i(n,s|h)}{2dl} \\
& - U_i(n-1,s) \frac{\bar{K}_i(n,s|h) - \bar{K}_i(n-2d,s|h)}{2dl} \Bigg] \Bigg\}. \qquad (4)
\end{aligned}
$$

As in section A.1, we now take the limit as $l, \tau \to 0$ and $n, s, h \to \infty$ such that $x = nl$, $t = s\tau$, $D = l^2/(2\tau)$ and $\delta = lh$ are kept constant at non-zero, finite values. We also let $c = 4dqD$. This leads to the following advection-diffusion equation

$$
\frac{\partial u_i}{\partial t} = D \frac{\partial^2 u_i}{\partial x^2} + c \frac{\partial}{\partial x} \left[u_i \frac{\partial \bar{k}_i}{\partial x} \right], \qquad (5)
$$

where

$$
\bar{k}_i(x,t) = \frac{1}{2\delta} \int_{-\delta}^{\delta} k_i(x+z,t) \mathrm{d}z. \qquad (6)
$$

For a detailed explanation of the limit result $\bar{K}_i(n,s) \to \bar{k}_i(x,t)$, see Potts and Lewis (2015).

We model agents as moving on the interval $[0, L]$. Therefore we need to impose a boundary condition on Equation (5). A biologically realistic choice is a zero-flux boundary condition, meaning that the migration rate into $[0, L]$ is equal to the migration rate out of $[0, L]$. This is given as follows

$$\left[D\frac{\partial u_i}{\partial x} + cu_i\frac{\partial \bar{k_i}}{\partial x}\right]\Bigg|_{x=0} = \left[D\frac{\partial u_i}{\partial x} + cu_i\frac{\partial \bar{k_i}}{\partial x}\right]\Bigg|_{x=L} = 0. \tag{7}$$

Since $u_i(x, t)$ is a probability density function, the initial conditions must integrate to 1 over the spatial domain. In other words

$$\int_0^L u_i(x, 0)dx = 1. \tag{8}$$

Equations (7) implies that the time-derivative of $\int_0^L u_i(x, t)dx$ is zero. This, combined with Equation (8), implies that

$$\int_0^L u_i(x, t)dx = 1, \tag{9}$$

for any $t \geq 0$. To account for the boundaries in the spatial averaging (Equation 6), we need to modify Equation (6) as follows

$$\bar{k_i}(x, t) = \begin{cases} \frac{1}{\delta+x}\int_{-x}^{\delta} k_i(x+z, t)\mathrm{d}z & \text{if } 0 < x < \delta, \\ \frac{1}{2\delta}\int_{-\delta}^{\delta} k_i(x+z, t)\mathrm{d}z & \text{if } \delta < x < L-\delta, \\ \frac{1}{\delta+L-x}\int_{-\delta}^{1-x} k_i(x+z, t)\mathrm{d}z & \text{if } L-\delta < x < L. \end{cases} \tag{10}$$

Then Equations (7), (9) and (10) are equivalent to Equations (7), (8) and (6) from the Main Text, respectively.

Supplementary Appendix B

Here we give some mathematical analysis of the dispersion relations shown in Figure 1 from the Main Text. The dispersion relation plots the dominant eigenvalues. For each κ, this is the value of σ with the greatest real part such that $\det(A-\sigma I)=0$. To determine whether patterns may form, we need to find out the parameter values for which there is some pair (κ,σ), with $\mathrm{Re}(\sigma)>0$, that solves $\det(A-\sigma I)=0$. The function $\det(A-\sigma I)$ is given as follows

$$\begin{aligned}
\det(A-\sigma I) &= a_4\sigma^4+a_3\sigma^3+a_2\sigma^2+a_1\sigma+a_0,\\
a_4 &= 1,\\
a_3 &= 2\left(\frac{m+b+1}{a}+\kappa^2\right),\\
a_2 &= \frac{(m+b+1)^2}{a^2}+\frac{4\kappa^2(m+b+1)}{a}+\kappa^4+\frac{2\gamma\kappa m\sin(\kappa\delta)}{\delta a(m+b+1)},\\
a_1 &= \frac{2\kappa^2(m+b+1)^2}{a^2}+\frac{2\kappa^4(m+b+1)}{a}+\frac{2\gamma\kappa^3 m\sin(\kappa\delta)}{\delta a(m+b+1)}+\frac{2\gamma\kappa m\sin(\kappa\delta)}{\delta a^2},\\
a_0 &= \frac{\delta^2\kappa^4(m+b+1)^4+2\gamma\delta\kappa^3 m(m+b+1)^2\sin(\kappa\delta)-\gamma^2\kappa^2 b(b+2m)\sin^2(\kappa\delta)}{\delta^2a^2(m+b+1)^2}.
\end{aligned} \tag{11}$$

The Routh-Hurwitz formulae (Routh, 1877; Hurwitz, 1895) give the following necessary and sufficient criteria for the real parts of σ to be below zero

$$\begin{aligned}
a_i > 0, &\text{ for all } i=0,1,2,3,4,\\
a_3a_2 &> a_4a_1,\\
a_3a_2a_1 &> a_4a_1^2+a_3^2a_0.
\end{aligned} \tag{12}$$

In fact, for all the plots in Figure 1 from the Main Text, the dominant eigenvalues are real. In such cases, $\sigma\in\mathbb{R}_{\le 0}$. Therefore it makes sense to analyse the places where $\sigma=0$. Here, equation (11) becomes $\det(A)=a_0$, so we look for the places where $a_0>0$.

First note that we cannot have $\kappa=0$ if $a_0>0$. Dividing a_0 by κ^2, and noting that the denominator of a_0 is positive, we have

$$\delta^2\kappa^2(m+b+1)^4 + 2\gamma\delta\kappa m(m+b+1)^2\sin(\kappa\delta) - \gamma^2 b(b+2m)\sin^2(\kappa\delta) > 0. \tag{13}$$

This rearranges to give the following (using the fact that $\kappa, \delta \neq 0$)

$$-\frac{(m+b+1)^2}{\gamma(b+2m)} < \frac{\sin(\kappa\delta)}{\kappa\delta} < \frac{(m+b+1)^2}{\gamma b}, \tag{14}$$

where the right-hand inequality is only valid when $b \neq 0$.

In the case $b = 0$, examined in Figure 1f from the Main Text, the only valid inequality from (14) is

$$\frac{\sin(\kappa\delta)}{\kappa\delta} > -\frac{(m+1)^2}{2\gamma m}. \tag{15}$$

Since the minimum of $\sin(x)/x$ is $-2/(3\pi)$, obtained where $x = 3\pi/2$, we only obtain values of κ for which Equation (15) holds when $(m+1)^2/(2\gamma m) > 2/(3\pi)$. Away from this, there may exist eigenvalues with non-negative real parts. In other words, patterns may only form if $(m+1)^2/(2\gamma m) < 2/(3\pi)$.

The set of κ for which Equation (15) fails to hold (i.e. patterns may form) is a subset of the set $S = \{\kappa : \sin(\kappa\delta) < 0\}$. Since $S = \{\kappa : (2n+1)\pi < \kappa\delta < (2n+2)\pi \, n \in \mathbb{Z}\}$, the lowest possible wavenumbers at which patterns may form if $b = 0$ (if they form at all) must be within the range $\kappa \in (\pi/\delta, 2\pi/\delta)$.

Patterns that correspond to territories (i.e. with $u_{1*}(x)$ concentrated mainly on the left-hand side of $[0,1]$ and $u_{2*}(x)$ on the right-hand side) occur in the range of wavenumbers $\kappa \in [\pi, 2\pi]$. Hence δ must be close to 1 for such territorial patterns to form. In other words, agents must respond to a spatial averaging across almost the entire terrain for territorial patterns to form when $b = 0$. This is likely to be biologically unrealistic, so we conclude that $b > 0$ is necessary for territorial patterns to form in realistic scenarios.

Supplementary Appendix C

A feature of the plots in figure 1f from the Main Text is that patterns (albeit biologically unrealistic ones) may form for a set of wavenumbers that is bounded below by a non-zero value of κ. Here we examine the nature of the bifurcations suggested by figure 1f from the Main Text. Bifurcations occur when the following all hold

$$\det(A-\sigma I)=0, \tag{16}$$

$$\mathrm{Re}(\sigma')\leq \mathrm{Re}(\sigma), \text{ for all eigenvalues } \sigma' \tag{17}$$

$$\mathrm{Re}(\sigma)=0, \tag{18}$$

$$\sigma \text{ is a local maximum,} \tag{19}$$

where A is as in Equation (21) from the Main Text. Condition (16) just says that σ is an eigenvalue, and (17) that σ is the dominant eigenvalue. Condition (18) says that σ lies on the horizontal axis of the dispersion relation curve (e.g. Figure 1 from the Main Text). Together with conditions (16-18), Condition (19) means that σ is at the bifurcation point between stability and instability of the constant solution to Equations (10-13) from the Main Text.

The full expression for $\det(A-\sigma I)$ is given in Equation (11). Differentiating this by κ and setting $\mathrm{d}\sigma/\mathrm{d}\kappa=0$ (to partially fulfill Condition 19), we have

$$\begin{aligned}
0 =&4\kappa\sigma^3+\left\{4\kappa^3+8\kappa\frac{m+b+1}{a}+\frac{2\gamma m}{\delta a(m+b+1)}\left[\sin(\kappa\delta)+\kappa\delta\cos(\kappa\delta)\right]\right\}\sigma^2\\
&+\left\{8\kappa^3\frac{m+b+1}{a}+4\kappa\left(\frac{m+b+1}{a}\right)^2+\frac{4\gamma\kappa^2 m\sin(\kappa\delta)}{a\delta(m+b+1)}\right.\\
&\left.\quad+\left[\frac{2\gamma\kappa^2 m}{a\delta(m+b+1)}+\frac{2\gamma m}{a^2\delta}\right]\left[\sin(\kappa\delta)+\kappa\delta\cos(\kappa\delta)\right]\right\}\sigma\\
&+\left\{4\kappa^3\left(\frac{m+b+1}{a}\right)^2+\frac{4\gamma\kappa^2 m\sin(\kappa\delta)}{a^2\delta}-\frac{2\kappa\gamma^2\sin^2(\kappa\delta)(2mb+b^2)}{a^2\delta^2(m+b+1)^2}\right.\\
&\left.\quad-\frac{\gamma^2\kappa^2\sin(2\kappa\delta)(2mb+b^2)}{a^2\delta(m+b+1)^2}+\frac{2\gamma m\kappa^2}{a^2\delta}\left[\sin(\kappa\delta)+\kappa\delta\cos(\kappa\delta)\right]\right\}.
\end{aligned} \tag{20}$$

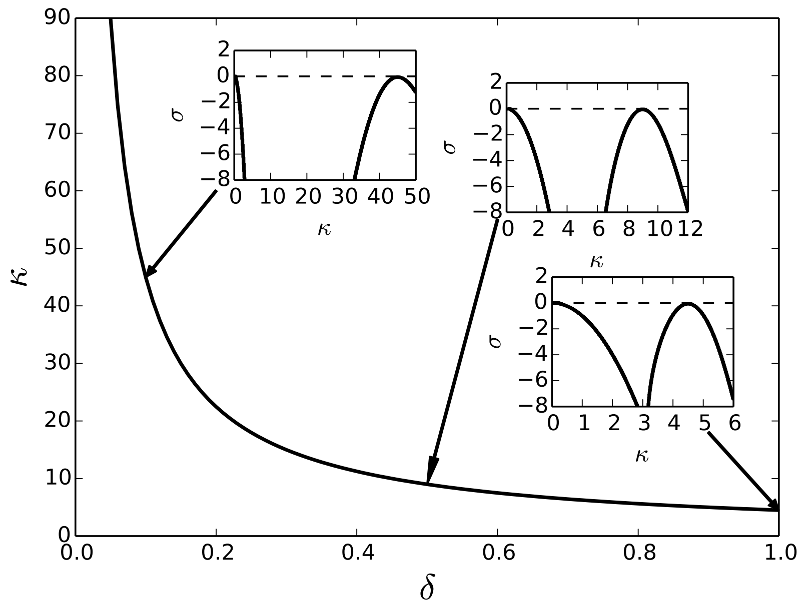

Fig. 1. Bifurcation points when $b = 0$. Parameter values for which the system described by Equations (10-13) from the Main Text goes through a bifurcation, in the case when $b = 0$, $\gamma = 100$, and $a = 0.1$. The value of m is determined by the other parameters (see Supplementary Appendix C) and is equal to 0.024, to two significant figures, for each of the pairs (κ, δ) plotted here. Insets show the dispersion relations for $\delta = 0.1, 0.5, 1$ from top to bottom, respectively.

We wish to show that the bifurcation points implied by Figure 1f from the Main Text occur where $\mathrm{Im}(\sigma) = 0$, so that the unstable range does not have oscillatory solutions. In other words, the Turing bifurcations are not also Hopf bifurcations [see e.g. Baurmann et al. (2007) for explanation of this terminology]. In this case, Equation (18) means that $\sigma = 0$, so we require the following to hold

$$\begin{aligned} 0 =& 4\kappa^3(m+b+1)^2 + \frac{4\gamma\kappa^2 m \sin(\kappa\delta)}{\delta} - \frac{2\kappa\gamma^2\sin^2(\kappa\delta)(2mb+b^2)}{\delta^2(m+b+1)^2} \\ & - \frac{\gamma^2\kappa^2\sin(2\kappa\delta)(2mb+b^2)}{\delta(m+b+1)^2} + \frac{2\gamma m\kappa^2}{\delta}\left[\sin(\kappa\delta) + \kappa\delta\cos(\kappa\delta)\right]. \end{aligned} \tag{21}$$

Notice that Equation (21) is independent of a, which explains why all the dispersion relations in Figure 1d from the Main Text cross the horizontal axis at the same point.

One (trivial) solution to Equation (21) is $\kappa = 0$. Away from this, and in the case $b = 0$, pertinent to Figure 1f from the Main Text, Equation (21) becomes

$$4\kappa\delta m^2 + [6\gamma\sin(\kappa\delta) + 2\gamma\kappa\delta\cos(\kappa\delta) + 8\kappa\delta]m + 4\delta\kappa = 0. \tag{22}$$

To apply condition (16), we use Equation (11) and set $b = 0$ and $\sigma = 0$. Assuming $\kappa, \gamma, \delta, m \neq 0$, this rearranges to give

$$\frac{\sin(\kappa\delta)}{\kappa\delta} = -\frac{(m+1)^2}{2\gamma m}. \tag{23}$$

Bifurcation points then arise when (i) both Equations (22) and (23) are satisfied, (ii) the turning point on the graph of $\mathrm{Re}(\sigma)$ against κ is a maximum, (iii) there are no other eigenvalues with larger real part. Since the aim is to understand Figure 1f from the Main Text, we fix $\gamma = 0$ and $a = 0.1$ then search for values of κ and m that satisfy Equations (22) and (23) for $\delta = 0.01, 0.02, \ldots, 1$. Conditions (ii) and (iii) are then checked numerically. The resulting curve of κ versus δ is shown in Figure 1.

Supplementary Appendix D

The numerical algorithm from section 3.2 from the Main Text uses a forward-difference approximation for time and central difference for space. The interval $[0, 1]$ is divided into 100 equal and non-overlapping sections and iterations are performed every 10^{-5} time steps. The algorithm is stopped when all the values of $u_1(x, t)$ and $u_2(x, t)$ are increasing by less than 10^{-8} each iteration. At time $t = 0$, $u_1(x, 0) = 100$ for $x \in [0.25, 0.26]$ and $u_1(x, 0) = 0$ elsewhere. Also, $u_2(x, 0) = 100$ for $x \in [0.75, 0.76]$ and $u_1(x, 0) = 0$ elsewhere.

Supplementary Appendix E

Here, we examine whether there are non-constant solutions to Equations (22-25) from the Main Text. We prove mathematically that they do not exist when $m = 0$ and give numerical evidence to show that this holds for $m > 0$.

Equations (22-25) from the Main Text lead to the following equations for the steady-states u_{i*} and k_{i*} of u_i and k_i respectively

$$0 = u_{1*}u_{2*}(1 - k_{i*}) - k_{i*}(m + bu_{i*}), \tag{24}$$

$$0 = \frac{\mathrm{d}u_{i*}}{\mathrm{d}x} + \gamma u_{i*}\frac{\mathrm{d}k_{i*}}{\mathrm{d}x}. \tag{25}$$

Henceforth in this section we drop the asterisks and, unless necessary, drop the explicit dependence upon x for ease of notation. Equation (24) implies that

$$k_i = \frac{u_1 u_2}{m + bu_i + u_1 u_2}. \tag{26}$$

Differentiating equation (26) with respect to x, rearranging so that $\mathrm{d}k_i/\mathrm{d}x$ is the subject, and plugging the result into equation (25) gives the following

$$
\begin{aligned}
&B\dot{\mathbf{u}} = 0,\\
&B = \begin{pmatrix} b_{11} & b_{12} \\ b_{21} & b_{22} \end{pmatrix},\\
&b_{11} = (m + bu_1 + u_1u_2)^2 + \gamma u_1u_2(m + bu_1 + u_1u_2) - \gamma u_1^2u_2(b + u_2),\\
&b_{12} = \gamma u_1^2(m + bu_1 + u_1u_2) - \gamma u_1^3u_2,\\
&b_{21} = \gamma u_2^2(m + bu_2 + u_1u_2) - \gamma u_1u_2^3,\\
&b_{22} = (m + bu_2 + u_1u_2)^2 + \gamma u_1u_2(m + bu_2 + u_1u_2) - \gamma u_1u_2^2(b + u_1),\\
&\dot{\mathbf{u}} = \begin{pmatrix} \mathrm{d}u_1/\mathrm{d}x \\ \mathrm{d}u_2/\mathrm{d}x \end{pmatrix}.
\end{aligned} \tag{27}
$$

E.1 The case $m = 0$

First, we analyse Equations (27) exactly in the case $m = 0$. In this case, we have

$$
\begin{aligned}
b_{11} &= u_1^2(b + u_2)^2,\\
b_{12} &= \gamma b u_1^3,\\
b_{21} &= \gamma b u_2^3,\\
b_{22} &= u_2^2(b + u_1)^2,
\end{aligned} \tag{28}
$$

Then $\det(B) = 0$ means that $u_1 = 0$ or $u_2 = 0$ or

$$(b + u_2)^2(b + u_1)^2 - \gamma^2b^2u_1u_2 = 0. \tag{29}$$

We claim that the Equation (29) has no real-valued solutions. Placing u_1 as the subject, we have

$$
\begin{aligned}
u_1 &= \frac{\gamma^2 b^2 u_2}{2(b+u_2)^2} - b \pm \sqrt{-D_1 D_2 D_3}, \\
D_1 &= \frac{\gamma^2 b^3 u_2}{4(b+u_2)^4}, \\
D_2 &= \left[u_2 + \frac{(8-\gamma^2)b}{8} + \frac{b\sqrt{(8-\gamma^2)^2 - 64}}{8} \right], \\
D_3 &= \left[u_2 + \frac{(8-\gamma^2)b}{8} - \frac{b\sqrt{(8-\gamma^2)^2 - 64}}{8} \right]. \qquad (30)
\end{aligned}
$$

D_1 is always real and positive, by construction. If $(8-\gamma^2)^2 - 64 \geq 0$ then D_2 and D_3 are real and positive, so the solutions for u_1 are not real. If $(8-\gamma^2)^2 - 64 < 0$ then

$$
D_2 D_3 = \left(u_2 + \frac{(8-\gamma^2)b}{8} \right)^2 + \frac{b^2}{64}[64 - (8-\gamma^2)^2]. \qquad (31)
$$

Since $64 - (8-\gamma^2)^2 > 0$, the right-hand side of Equation (31) is positive. Hence $D_1 D_2 D_3 > 0$ so solutions for u_1 are not real, as claimed. Thus either $u_1 = 0$, $u_2 = 0$ or $\dot{\mathbf{u}} = 0$, so that when $m = 0$, the only classical solutions to Equation (27) are constant.

E.2 The case $m > 0$

Here, we analyse the phase plane of Equation (27) to give evidence for lack of non-constant steady-state solutions. Notice that either $\det(B) = 0$ or $\dot{\mathbf{u}} = 0$. In the latter case, the arrows on the phase portrait denoting $\dot{\mathbf{u}}$ vanish. We therefore plot the curves $\det(B) = 0$ (Figure 2) for the same sets of parameter values (b, γ, m) as examined in Figure 2 from the Main Text. We overlay arrows denoting the possible directions of $\dot{\mathbf{u}}$ at various points on these curves, were classical solutions to exist.

Notice that these arrows are almost never tangential to the curve. Assuming that this observation is true in general, the implication is that if a solution to Equation (27) has a point

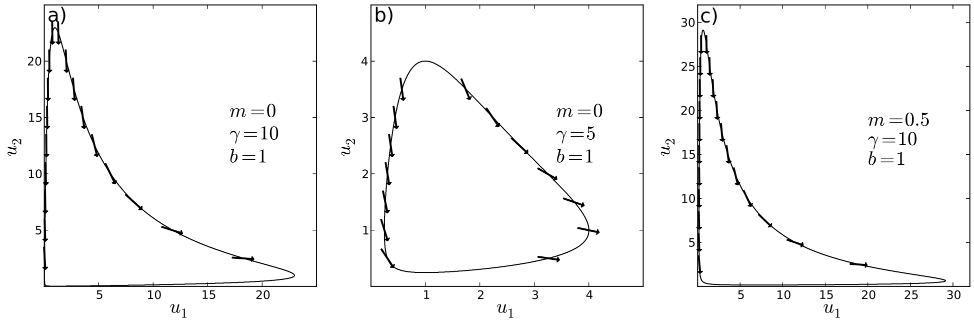

Fig. 2. Phase portraits in the case $\delta \to 0$. The curves denote the places where $\mathrm{d}u_1/\mathrm{d}x, \mathrm{d}u_2/\mathrm{d}x \neq 0$. The arrows denote the directions of the vector $(\mathrm{d}u_1/\mathrm{d}x, \mathrm{d}u_2/\mathrm{d}x)$ at certain places on these curves.

x where $[u_1(x), u_2(x)]$ is on the curve $\det(B) = 0$ then there is some c such that the points $[u_1(x \pm c'), u_2(x \pm c')]$ do not lie on the curve $\det(B) = 0$, for any $0 < c' < c$. In other words the curves u_1 and u_2 must have zero gradient almost everywhere (i.e. except possibly on a set of measure zero). No non-constant continuous functions have this property. It follows that any classical solution to the system in Equation (27) must be constant, as long as the observations from Figure (2) hold in general.

238 Supplementary Figures

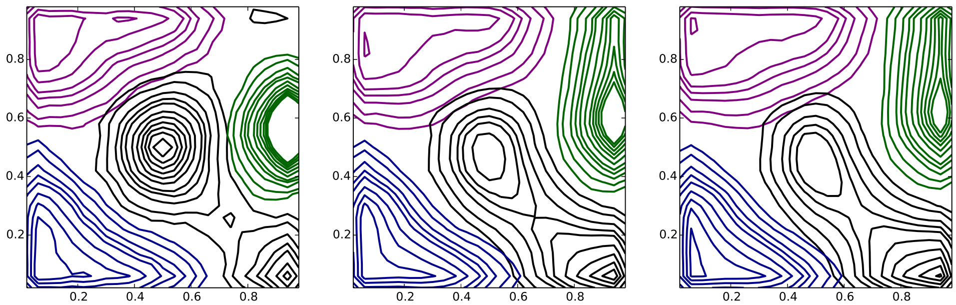

Fig. 3. Effect of increased time on territorial patterns in 2D IBM. In all of these plots, $d = 5$, $h = 5$, $q = 3$, $\rho = 1$, $\beta = 0.1$ and $\mu = 0$. The left-hand panel displays utilisation distributions found by averaging over 100,000 timesteps (after 100,000 burn-in, see Main Text). The middle panel uses 500,000 timesteps. The right-hand panel uses 1,000,000 time steps. Though some small change is observed, the territories are qualitatively similar after 100,000 timesteps.

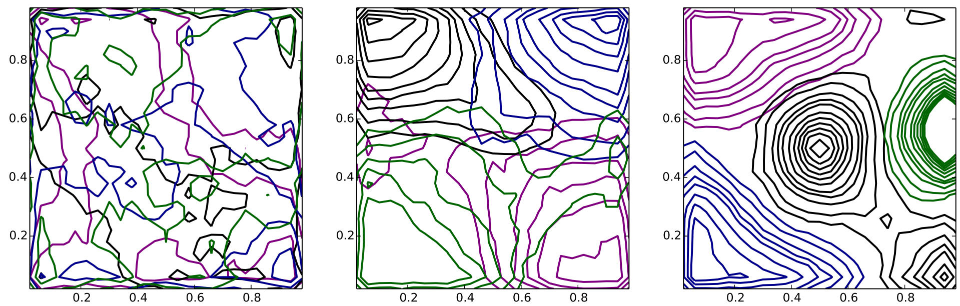

Fig. 4. Effect of increasing q on territorial patterns in 2D IBM. In all of these plots, $d = 5$, $h = 5$, $\rho = 1$, $\beta = 0.1$ and $\mu = 0$. The left-hand plot has $q = 1$, the middle has $q = 2$, and in the right-hand $q = 3$. As q is increased, we go from no clear territories to well-defined territories.

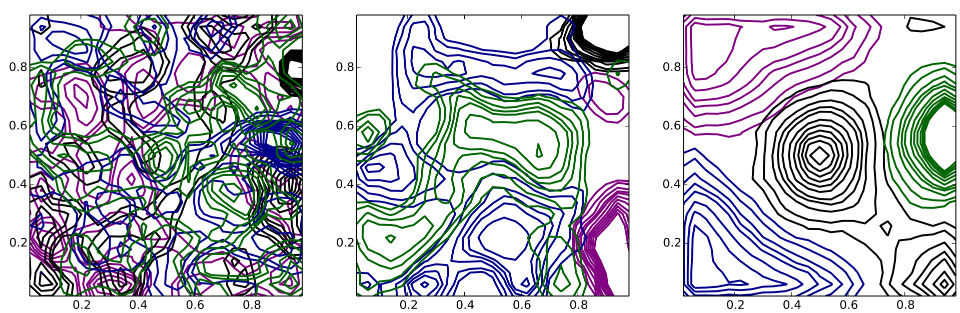

Fig. 5. Effect of increasing spatial averaging on territorial patterns in 2D IBM. In all of these plots, $q = 3$, $\rho = 1$, $\beta = 0.1$ and $\mu = 0$. The left-hand plot has $d, h = 1$, the middle has $d, h = 2$, and in the right-hand $d, h = 5$. As d and h decrease, the territorial structure becomes more fragmented. This concurs with the observation from figure 1c from the Main Text that lower spatial averaging means that instability is greatest at higher wave numbers.

References

Baurmann, M., T. Gross, and U. Feudel. 2007. Instabilities in spatially extended predator–prey systems: spatio-temporal patterns in the neighborhood of turing–hopf bifurcations. Journal of Theoretical Biology, **245**:220–229.

Hurwitz, A. 1895. Ueber die bedingungen, unter welchen eine gleichung nur wurzeln mit negativen reellen theilen besitzt. Mathematische Annalen, **46**:273–284.

Potts, J. R. and M. A. Lewis. 2015. Territorial pattern formation in the absence of an attractive potential. Journal of Mathematical Biology, **72**:25–46.

Routh, E. J. 1877. A treatise on the stability of a given state of motion: particularly steady motion. Macmillan and Company.